Spin transport properties of single metallocene molecules attached to single-walled carbon nanotubes via nickel adatoms

Peng Wei, Lili Sun, Enrico Benassi, Ziyong Shen, Stefano Sanvito, and Shimin Hou

Citation: The Journal of Chemical Physics **134**, 244704 (2011); doi: 10.1063/1.3603446
View online: http://dx.doi.org/10.1063/1.3603446
View Table of Contents: http://scitation.aip.org/content/aip/journal/jcp/134/24?ver=pdfcov
Published by the AIP Publishing

Spin transport properties of single metallocene molecules attached to single-walled carbon nanotubes via nickel adatoms

Peng Wei,[1] Lili Sun,[1] Enrico Benassi,[2] Ziyong Shen,[1] Stefano Sanvito,[3] and Shimin Hou[1,a)]

[1]*Key Laboratory for the Physics and Chemistry of Nanodevices, Department of Electronics, Centre for Nanoscale Science and Technology, Peking University, Beijing 100871, China*
[2]*Centro S3, CNR Istituto di Nanoscienze, 41125 Modena, Italy*
[3]*School of Physics and CRANN, Trinity College, Dublin 2, Ireland*

(Received 12 January 2011; accepted 5 June 2011; published online 28 June 2011)

The spin-dependent transport properties of single ferrocene, cobaltocene, and nickelocene molecules attached to the sidewall of a (4,4) armchair single-walled carbon nanotube via a Ni adatom are investigated by using a self-consistent *ab initio* approach that combines the non-equilibrium Green's function formalism with the spin density functional theory. Our calculations show that the Ni adatom not only binds strongly to the sidewall of the nanotube, but also maintains the spin degeneracy and affects little the transmission around the Fermi level. When the Ni adatom further binds to a metallocene molecule, its density of states is modulated by that of the molecule and electron scattering takes place in the nanotube. In particular, we find that for both cobaltocene and nickelocene the transport across the nanotube becomes spin-polarized. This demonstrates that metallocene molecules and carbon nanotubes can become a promising materials platform for applications in molecular spintronics. © *2011 American Institute of Physics*. [doi:10.1063/1.3603446]

I. INTRODUCTION

Organic spintronics is attracting growing interest as a new technological platform for cheap logic and memory devices at the end of the Si roadmap.[1,2] A promising strategy for constructing molecular spintronic devices is that of combining non-magnetic electrodes together with magnetic molecules, the latter being both the source of spin-polarized carriers and the tool for their manipulation.[2,3] Carbon nanotubes and, in particular, single-walled carbon nanotubes (SWCNTs) appear as an intriguing electrodes' material. When compared to traditional metals, such as Au and Pt, which are widely used in molecular electronic devices, SWCNTs have many advantages. First, the typical diameter of a SWCNT is around 1–2 nm, which is roughly the same as the size of many magnetic molecules. This means that ultrahigh device integration density can be, in principle, achieved in future integrated circuits incorporating SWCNTs electrodes. Second, nearly perfect SWCNTs can be routinely synthesized by using arc discharge, laser ablation, or chemical vapor deposition,[4] so that they are easily available in large quantities. Third, SWCNTs have been already successfully employed as electrodes for molecular junctions,[5–7] and preliminary experimental results have shown that devices made with SWCNTs can perform better than those fabricated with traditional metal electrodes.[8] Finally and most crucial for spintronics, the spin-relaxation length in SWCNTs is extremely long, thus that nanotubes can be used as spin-conserving channels with ballistic transport characteristics.[9] For all these reasons, grafting an appropriate magnetic molecule on a SWCNT in order to construct a molecular spin-device with specific functionalities, good performance, and high thermal stability, is an important step forward in organic spintronics.[2,10]

Among the many potential magnetic molecules,[11–21] first-row transition metal multidecker clusters form an intriguing and important family, whose spin-polarization is dominated by the 3d electrons of the metal atoms. For example, the infinite iron-cyclopentadienyl ($[FeCp]_\infty$) molecular wire is predicted to be a half-metallic ferromagnet,[15–17] while finite Fe_nCp_{n+1} ($n > 2$) clusters exhibit a nearly perfect spin-filter effect when attached to platinum electrodes through Pt adatoms.[17] In contrast, the band structure of the infinite $[NiCp]_\infty$ wire is non-magnetic, although the magnetic moment of finite Ni_nCp_{n+1} clusters is a periodic function of the number of NiCp monomers. The spin-transport properties of such finite clusters can be tuned in a controllable way by changing the contact geometry.[18]

In this work we explore another possibility. We investigate the spin-transport properties of three small molecules, composed of two Cp rings and one transition metal atom, either iron, cobalt, or nickel (the molecules are called, respectively, ferrocene, cobaltocene, and nickelocene), and attached to the sidewall of an armchair SWCNT. Our study is carried out by employing the non-equilibrium Green's function (NEGF) formalism combined with the spin density functional theory (DFT) (i.e., the NEGF+DFT approach).[22–31] Instead of using organic linker groups, such as amide and pyrrolidine rings,[10,32] we consider Ni adatoms. Our calculations show that the Ni adatom not only binds to the sidewall of the (4,4) armchair SWCNT with a large binding energy, but also that it preserves the nanotube spin degeneracy and modifies little the transmission around the Fermi level (E_F). Because of the strong interaction between the Ni adatom and the adsorbed

a)Author to whom correspondence should be addressed. Electronic mail: smhou@pku.edu.cn.

metallocene molecules, the density of states (DOS) of Ni is modulated in a spin-dependent fashion by that of the molecule, thus that tunable spin-polarized transport across the nanotube can be realized when single cobaltocene and nickelocene molecules are attached.

II. CALCULATION METHOD

Geometry optimization and electronic structure calculations are performed by using the SIESTA package.[33] We employ improved Troullier-Martins pseudopotentials to describe the core electrons and the generalized gradient approximation (GGA) of Perdew, Burke, and Ernzerhof (PBE) for the exchange and correlation energy.[34,35] The wave-functions for the valence electrons are expanded over a finite range numerical basis set of double-zeta plus polarization quality for all elements, including H, C, Fe, Co, and Ni.[17,18] Furthermore, the basis set superposition error correction is included[36] when computing the binding energies of the Ni adatom and the metallocene molecules adsorbed on the sidewall of the (4,4) SWCNT. Geometry optimization is obtained by conjugate gradient relaxation until the forces are smaller than 0.03 eV $Å^{-1}$.

The spin-polarized transport calculations are performed by using the SMEAGOL package,[29–31] which is a practical implementation of the NEGF+DFT approach. Since SMEAGOL uses SIESTA as the DFT platform, we employ the same pseudopotentials, basis set, and GGA functional, for both the geometry relaxation and the transport. Considering the atomic and electronic structure of SWCNTs, a (4,4) armchair SWCNT is chosen as a representative electrode.[20,21,37] In the NEGF construction the charge density is integrated over 70 energy points along the semi-circle, 25 energy points along the line in the complex plane, and 20 poles in the Fermi distribution (the electronic temperature is 25 meV). The zero-bias transmission functions for the spin-up and spin-down electrons ($\sigma = \uparrow/\downarrow$) are calculated from the Landauer formula:

$$T_\sigma(E) = Tr[\Gamma_1 G_\sigma \Gamma_2 G_\sigma^+](E),$$

where G_σ is the spin-dependent retarded Green's function of the extended molecule (molecule of interest plus a portion of the electrodes) and $\Gamma_{1,2}$ are the broadening functions of the left- and right-hand side electrode. It should be noted here that the broadening functions $\Gamma_{1,2}$ are spin-independent since the semi-infinite SWCNT electrodes are not spin-polarized. More details about the numerical implementation can be found in recent literature.[29–31]

Our transport simulation cell comprises a 28.53 Å long portion of the SWCNT, which incorporates the absorption site, the Ni adatom, and the relevant molecule. This includes on total 192 C atoms. The electrodes are constructed with the same (4,4) nanotube which is present in the scattering region. This means that in the absence of scattering centers the transmission should be an integer corresponding to the number of nanotube open scattering channels.

III. RESULTS AND DISCUSSION

A. Atomic structure and electronic transport properties of a (4,4) armchair SWCNT with one adsorbed Ni adatom

When one Ni adatom adsorbs outside the sidewall of the (4,4) armchair SWCNT, the atop site is found to be the most stable binding position (see Fig. 1). In contrast to small organic functional groups, such as –COOH, $–NH_2$, and $–NO_2$ which also absorb at the atop site,[38] the Ni adatom does not sit directly above the connecting carbon atom but moves slightly towards the other two neighboring carbon atoms. Thus, the Ni–C bond direction is tilted by about 31.58° with respect to the SWCNT diameter passing through the connecting carbon atom. The shortest Ni–C bond length is optimized to be 1.840 Å, which is about 0.18 Å shorter

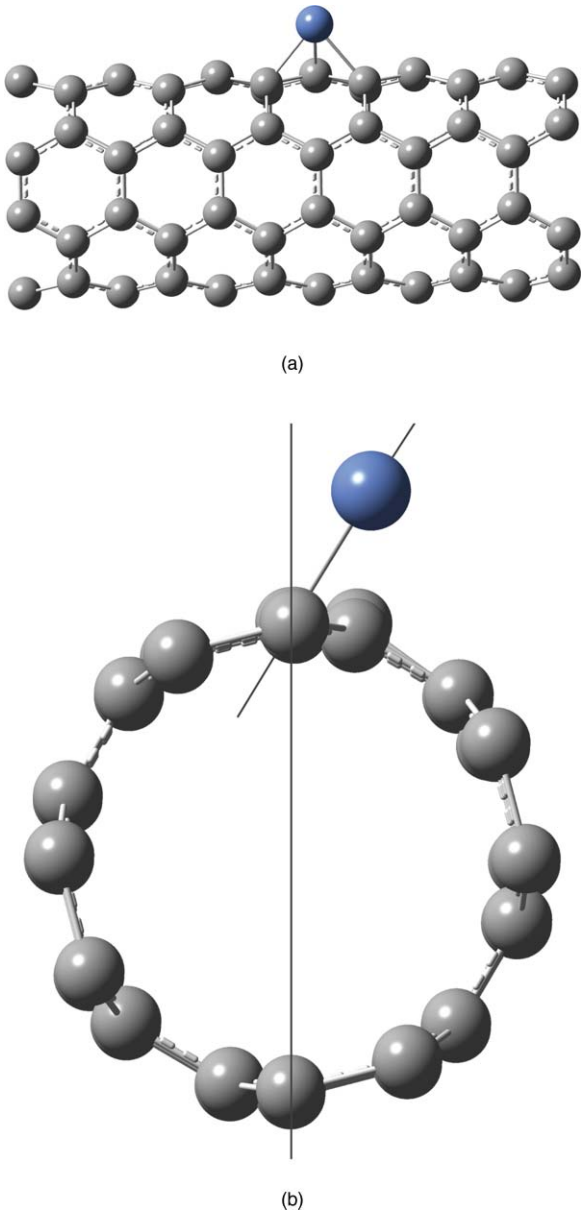

FIG. 1. Optimized geometric structure for a Ni adatom adsorbed at the outside atop site of a (4,4) armchair SWCNT: (a) side view and (b) cross section perpendicular to the tube axis.

than the distance (2.022 Å) between the Ni adatom and the two neighboring carbon atoms. The adsorbed Ni adatom turns out to be not spin-polarized despite the fact that an isolated Ni atom has a spin magnetic moment of $2\mu_B$, and that Mülliken population analysis shows little charge transfer between the Ni and the neighboring carbon atoms. These results are in good agreement with previous plane-wave DFT calculations.[39] The binding energy for the Ni adatom adsorbed at the atop site is calculated to be 1.72 eV, which is slightly smaller than the value (2.0 eV) reported previously.[39]

The adsorption of a Ni adatom does not change much the atomic structure of the (4,4) SWCNT around the adsorption site. In the pristine SWCNT the C–C bond distance is calculated to be 1.438 Å. The Ni adsorption elongates the bond lengths between the carbon atom at the bonding site and its three nearest-neighbors, respectively, to 1.479 Å, 1.479 Å, and 1.441 Å. This is a much more gentle modification than that occurring after adsorption, for instance, of a –COOH group at the atop site. In this second case, the same C–C bond lengths increase to 1.525 Å, 1.524 Å, and 1.540 Å, leading to an $sp^2 \rightarrow sp^3$ transition for the connecting carbon atom and simultaneously a large decrease of the transmission around the Fermi level.[38]

In Fig. 2(a), we present the zero-bias transmission coefficient for the (4,4) armchair SWCNT/Ni adatom system. We find that not only the electron transmission is spin-degenerate along the entire energy range, but also that $T(E_F)$ is not perturbed by the presence of the Ni adatom. This happens despite the fact that five transmission dips, reducing $T(E)$ by about one, appear, respectively, at −1.39 eV, −0.90 eV, −0.39 eV, −0.33 eV, and 0.54 eV. The reductions in the transmission can be understood by looking at the DOS projected over the Ni adatom. As one can see in Fig. 2, there is a one-to-one correspondence between the peaks in the DOS and the dips in $T(E)$, meaning that the electron scattering is generated by the interaction between the two low-energy SWCNT bands and the Ni atomic orbitals. Going into more details, we observe that the transmission dip at 0.54 eV is mainly caused by the Ni 4s and 4p atomic orbitals, while the other four dips below E_F are due to the Ni 3d orbitals. Although the electronic configuration of an isolated Ni atom is $[Ar]3d^8 4s^2$, the 4s level of the adsorbed Ni adatom lies predominantly above the Fermi level and remains thus unoccupied, whereas the 3d orbitals are located below E_F and are almost completely filled. More importantly, the Ni adatom does not assume the 2+ configuration, but remains charge neutral. In order to achieve charge neutrality, the 4s electrons are promoted into the 3d shell and thus the Ni spin moment is quenched. This contrasts the case of Fe adatoms on SWCNTs,[40] which remain magnetic and cause scattering mostly in the minority band.

In a pristine armchair SWCNT there are two open conducting channels per spin in a rather large energy range around E_F corresponding to the two linear bands crossing E_F.[41] One of them has a π-bonding character, while the other is π-antibonding (π^*) in nature. The π state is even and the π^* state is odd under the reflection symmetry operations with respect to the mirror planes containing the tube axis.[42] It is then interesting to examine whether the reduction in transmission due to the Ni adatom is even in the two channels or interests only one of them (for a complete analysis see Table I). Although the eigenchannel analysis[43–45] shows that at all the five transmission dips, one conducting channel remains fully open, while the other is completely blocked, the orbital contribution to the open channel (either π or π^*) is different. For example, the open conducting channel at 0.54 eV (−1.39 eV)

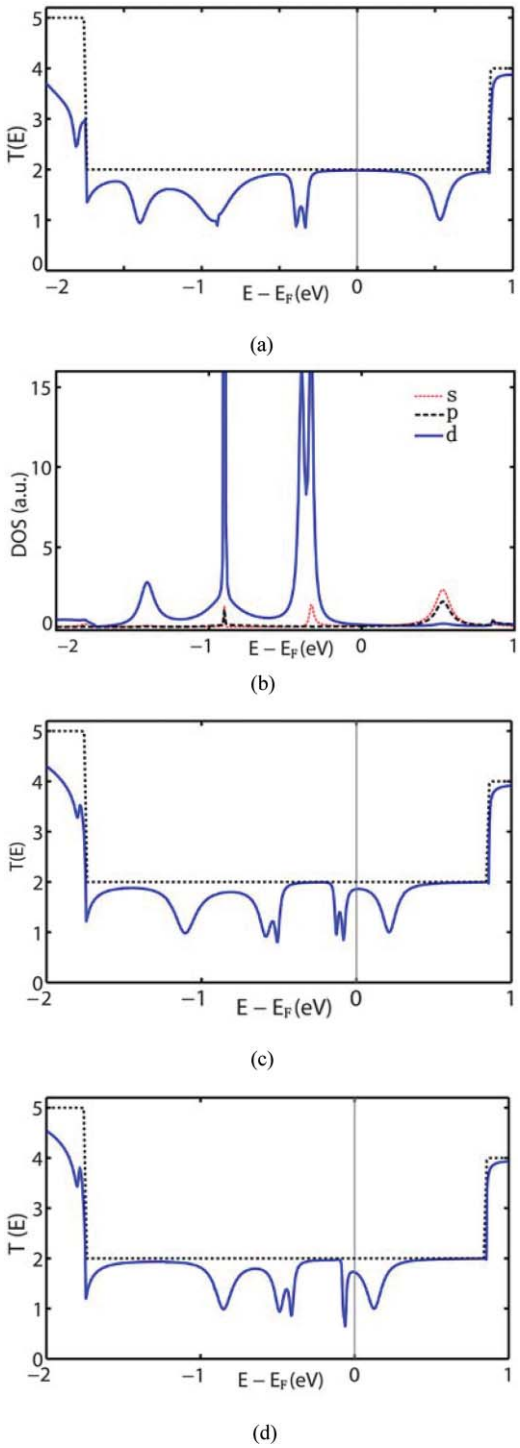

FIG. 2. Transport properties of a (4,4) armchair SWCNT with an adsorbed Ni adatom: (a) the zero-bias transmission spectrum for both the pristine tube (dashed line) and the tube after the Ni adsorption (solid line), here only the spin-up channel is shown due to the spin-degeneracy; and (b) the projected DOS for the Ni adatom. Panels (c) and (d) report the zero-bias transmission spectrum for the two additional configurations where the Ni atom sits on top of the linking C, respectively, at 1.84 Å (c) and 2.0 Å (d).

TABLE I. Scattering-state decomposition of the transmission over the nanotube π and π^* channels. $T_{\alpha\to\beta}$ is the contribution to the transmission coefficient for scattering from the α to the β channel (note that $\pi\to\pi^*$ and $\pi^*\to\pi$ are equivalent). The energies selected correspond those where T deviates significantly from the integer value of a pristine nanotube. The second column in the table is for the optimized structure of Fig. 1, while the remaining ones are for a hypothetical configuration where the Ni adatom is absorbed directly above the linking carbon atom. In this second situation the third column is for a C–Ni distance of 1.84 Å, while the fourth column is for a distance of 2.0 Å.

	I					II						III			
E–E_F (eV)	−1.39	−0.90	−0.39	−0.33	0.54	−1.11	−0.59	−0.51	−0.13	−0.08	0.21	−0.85	−0.48	−0.41	0.13
$T_{\pi\to\pi}$	0.88	0.15	0.03	0.78	0.04	0.11	0.17	0.35	0.19	0.04	0.13	0.12	0.27	0.25	0.10
$T_{\pi^*\to\pi^*}$	0.00	0.23	0.74	0.00	0.65	0.43	0.30	0.07	0.34	0.52	0.41	0.42	0.19	0.16	0.47
$T_{\pi\to\pi^*}$	0.03	0.26	0.06	0.03	0.16	0.22	0.22	0.19	0.22	0.14	0.23	0.22	0.24	0.24	0.22

is almost completely dominated by the π^* (π) state, whereas both π and π^* almost equally contribute to the channel at −0.90 eV.

Such a selective orbital contribution to the transmission can be understood from the occurrence of band splitting and band mixing in the band structure of the (4,4) SWCNT decorated with a periodic array of Ni adatoms (see Fig. 3).[46] For instance, for an energy 0.5 eV above the Fermi level, band splitting induced by the adatom occurs in both the π and π^* bands. However, the magnitude of the π band splitting is much larger than that of the π^* one, indicating a larger interaction between the nanotube π-band and the Ni 4s and 4p atomic orbitals. The situation is a little different at about 1.5 eV below the Fermi level, where an energy band with an obvious π-bonding character appears. In contrast, at around −1.0 eV the π and π^* bands mix completely due to their strong interaction with the Ni 3d atomic orbitals and form together the open conducting channel at –0.90 eV. Notably, around the Fermi level both the π and π^* bands survive the adsorption of the Ni adatom and thus the two conducting channels remain open at E_F.

The degree of interaction between a foreign atom and the electronic structure of a nanotube is largely driven by the relative symmetry of the interacting orbitals.[40] An analysis based solely on symmetry, however, is not possible in our case since the Ni adatom does not occupy a high symmetry position over the nanotube lattice. This means that channel mixing is present. In order to demonstrate that the absorption position plays an important role in determining the transmission properties, in Figs. 2(c) and 2(d) we report the zero-bias transmission coefficient for a situation where the Ni adatom is directly above the binding carbon atom. In Fig. 2(c) the bonding distance is 1.84 Å, while it is 2.0 Å in Fig. 2(d). These figures, whose corresponding scattering-state analysis is reported in Table I, show that although the transmission dips are preserved across the different structures, their intensity and position can be modified by moving the exact bonding site. In particular, we note that the double-dip just below the Fermi level for the structure in Fig. 2(c) is merged into a single one as the Ni–C distance increases from 1.84 Å to 2.0 Å, i.e., when Fig. 2(c) is compared with Fig. 2(d). This indicates that not only the symmetry but also the precise bond length plays an important role here.

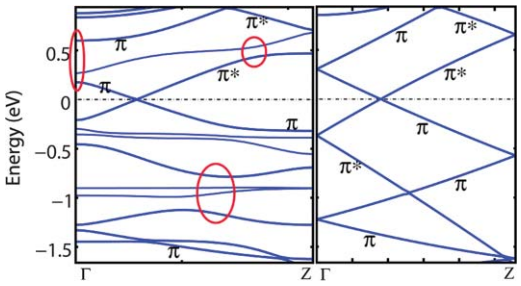

FIG. 3. Band structure along the nanotube axis direction for (a) the (4,4) SWCNT adsorbed with one Ni adatom and (b) the bare (4,4) SWCNT. The supercell dimension along the nanotube axis is 6 nanotube unit-cell lengths.

B. Spin transport properties of single metallocene molecules attached to a (4, 4) SWCNT through one Ni adatom

We now move to investigate the transport properties of single metallocene molecules. Since the electronic structure of metallocenes in the staggered configuration is essentially identical to that of the eclipsed one,[15,17,18] for the sake of brevity only the eclipsed configuration has been considered in our study. First, we connect a ferrocene to the sidewall of the (4,4) SWCNT through the Ni adatom (see Fig. 4(a)). In the gas-phase, ferrocene has a D_{5h} symmetry, with the five carbon atoms in each Cp ring being coplanar. The Fe–C bond length is optimized to be 2.07 Å.[17] After the ferrocene molecule is adsorbed onto the SWCNT sidewall the five carbon atoms in the inner Cp ring move slightly out of their plane due to the interaction with the Ni adatom. The average Fe–C bond lengths with the outer and inner Cp rings are shortened to 2.050 Å and 2.055 Å, respectively. Furthermore, the average bond length between the Ni adatom and the carbon atoms in the inner Cp ring is 2.169 Å, with the shortest and longest Ni–C bonds being, respectively, 2.138 Å and 2.196 Å. Since the adsorption of ferrocene weakens the coupling between the bonding Ni atom and the SWCNT, the Ni–C bond to the SWCNT is elongated to 1.882 Å. Finally, the binding energy for the ferrocene molecule to the nanotube through the Ni adatom is determined to be 1.61 eV. We have also checked, by performing calculations for the molecule attached to a single Ni atom, that the zero-point energy is only about 5% of the binding energy, so that it does not contribute significantly to the bond stability.

In Fig. 4(b), we present the equilibrium transmission spectrum of the SWCNT/ferrocene system. We find that, when compared to the case of a simple adsorbed Ni (see Fig. 2(a)), the ferrocene molecule does not significantly

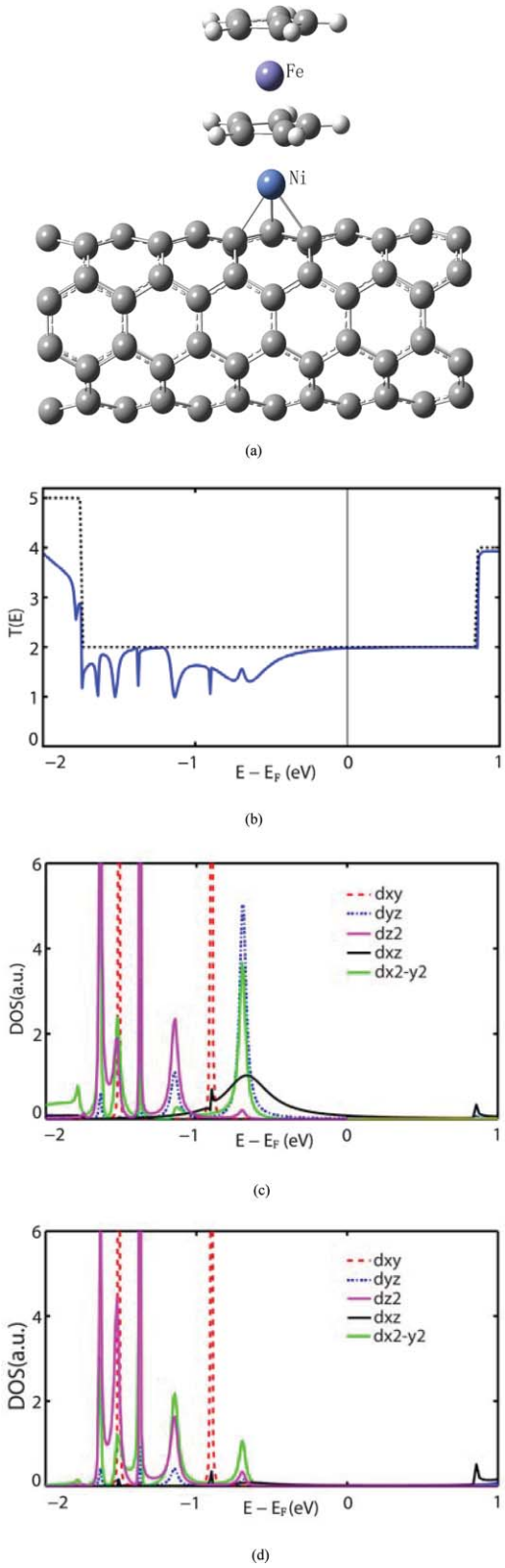

FIG. 4. Electronic and transport properties of a (4,4) armchair SWCNT with a ferrocene molecule adsorbed at its sidewall through a Ni adatom: (a) Optimized geometric structure and (b) the zero-bias transmission spectrum (solid line) for the spin-up or spin-down electrons. The transmission spectrum for the pristine SWCNT (dashed line) is also given for comparison. In (c) we present the DOS associated to the 3d atomic orbitals of the Ni adatom and in (d) that of the 3d atomic orbitals of the Fe center.

modify *T(E)*, i.e., the transmission still remains spin-degenerate over the entire energy range and approaches $T = 2$ around E_F. Certainly, modifications are present, such as the appearance of additional transmission dips far below the Fermi level and the suppression of the transmission dip at 0.54 eV [*T(E)* for $E > E_F$ is essentially identical to that of a pristine (4,4) SWCNT]. These two features can be traced back to the changes of the Ni DOS induced by the adsorption of the ferrocene molecule (Fig. 4(c)). We note that the Ni 3d contribution to the DOS splits into six well-separated peaks below the Fermi level. At the same time the Ni 4s and 4p orbitals are shifted further upward in energy and disappear from the energy window investigated here (where the pristine SWCNT has a transmission of two). Although the DOS of the iron center in ferrocene, shown in Fig. 4(d), resembles that of the Ni adatom, the six peaks in the DOS below E_F originate only from the Fe $3d_{xy}$, $3d_{x^2-y^2}$, and $3d_{z^2}$ atomic orbitals, while the Fe $3d_{xz}$ and $3d_{yz}$ contribution to the DOS is located at about 1.0 eV above the Fermi level. Since the ground state of an isolated ferrocene molecule is a singlet and the molecular states mainly composed of the Fe $3d_{xy}$, $3d_{x^2-y^2}$, and $3d_{z^2}$ orbitals are completely filled, whereas those dominated by the Fe $3d_{xz}$ and $3d_{yz}$ orbitals are empty,[17] we conclude that the adsorption of ferrocence onto the (4,4) SWCNT through the Ni adatom only affects slightly the Fe 3d occupation.

Next, we connect a cobaltocene to the nanotube. Although the adsorption structure of cobaltocene is almost the same as that of ferrocene, its effects on the transport properties of the nanotube are significantly different. As shown in Fig. 5(a), the most striking feature is that the adsorption of cobaltocene makes the transmission spin-polarized. In particular, in the energy range [−0.19 eV, 0.84 eV], *T(E)* for spin-up electrons first shows two transmission dips at −0.03 eV and 0.38 eV and then increases and approaches the value of two. In contrast, the only transmission dip for spin-down electrons occurs at around 0.72 eV. It can be expected that in this situation the DOS of the Ni adatom also becomes spin-polarized (see Fig. 5(b)). This is not the case for the energy range [−2.0 eV, −0.19 eV], but for higher energies spin-polarization appears. The spin-up Ni $3d_{yz}$ and $3d_{xz}$ atomic orbitals contribute, respectively, to the two DOS peaks centered at −0.03 eV and 0.38 eV. These, together with the Ni 4p shell, are sufficient to block completely one of the conduction channels of the nanotube, thus producing the two transmission dips around E_F. In contrast, the peaks in the spin-down DOS originating from the Ni 3d orbitals are all located below −0.5 eV, while the DOS peak centered at 0.76 eV is dominated by the Ni 4p orbitals.

Clearly, the spin polarization of both the nanotube transmission and the DOS of the Ni adatom can be attributed to the adsorption of the cobaltocene molecule. Similar to ferrocene, the gas-phase cobaltocene molecule also has an atomic structure with the D_{5h} symmetry. However, the ground-state electronic structure of cobaltocene is spin-polarized with a spin moment of $1\mu_B$, since Co has one valence electron more than Fe. The adsorbed cobaltocene molecule retains its spin polarization, which can be seen clearly from the DOS of the cobalt atom presented in Fig. 5(c). For the spin-up electrons, the two sharp peaks in the DOS centered at −0.03 eV and

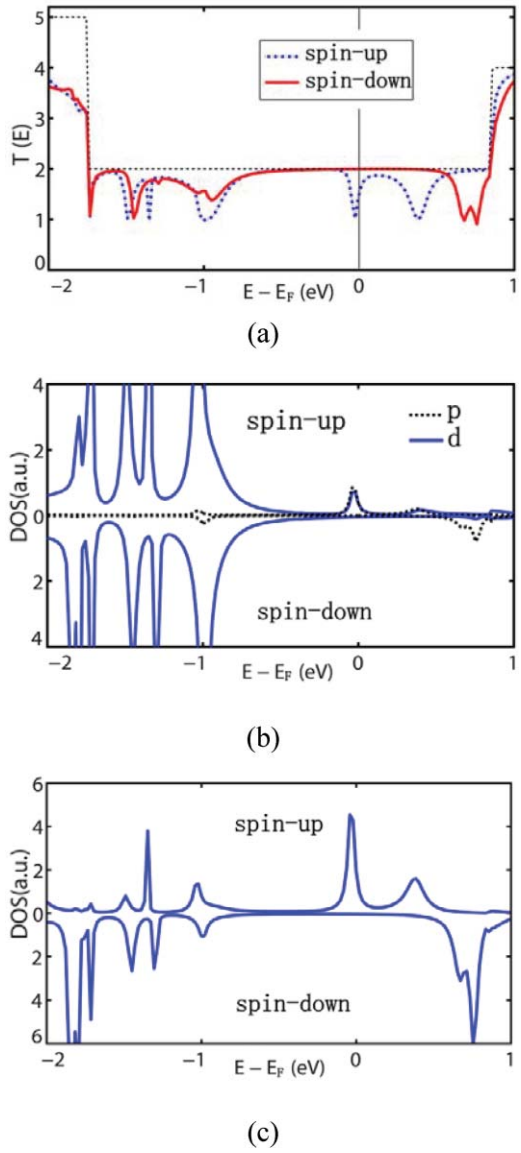

FIG. 5. Electronic and transport properties of a (4,4) armchair SWCNT with a cobaltocene molecule adsorbed at its sidewall through a Ni adatom: (a) The spin-resolved zero-bias transmission spectra, the blue dotted line for the spin-up electrons and the red solid line for the spin-down electrons. The transmission spectrum for the pristine SWCNT (dashed line) is also given for comparison. In (b) we present the DOS associated to the 3d atomic orbitals of the Ni adatom and in (c) that of the 3d atomic orbitals of the Co center.

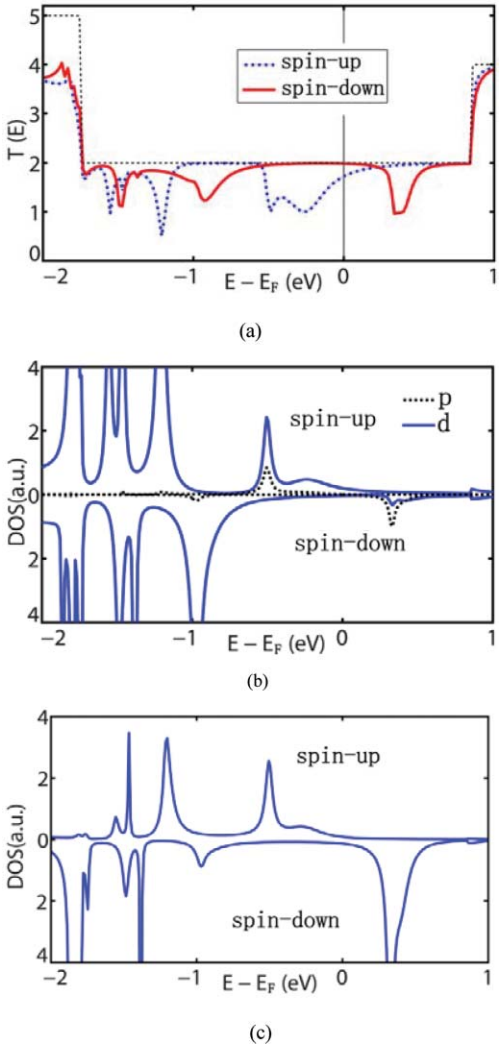

FIG. 6. Electronic and transport properties of a (4,4) armchair SWCNT with a nickelocene molecule adsorbed at its sidewall through a Ni adatom: (a) The spin-resolved zero-bias transmission spectra, the blue dotted line for the spin-up electrons and the red solid line for the spin-down electrons. The transmission spectrum for the pristine SWCNT (dashed line) is also given for comparison. In (b) we present the DOS associated to the 3d atomic orbitals of the Ni adatom and in (c) that of the 3d atomic orbitals of the Ni center.

0.38 eV originate from the Co $3d_{yz}$ and $3d_{xz}$ atomic orbitals, respectively. In contrast, the spin-down DOS peak dominated by the Co $3d_{yz}$ and $3d_{xz}$ atomic orbitals is centered at 0.76 eV. Due to the strong interaction between the Ni adatom and the cobaltocene molecule (the binding energy is calculated to be 1.89 eV), the DOS of the Ni adatom becomes spin-polarized and forms peaks at these corresponding energies. This modulates the spin transport properties across the (4,4) SWCNT.

Then we investigate the case of nickelocene. The corresponding spin-resolved transmission spectra are shown in Fig. 6(a). Among these three metallocene molecules, the modulation of nickelocene on the transport across the nanotube is the largest, since the transmission spectrum of the spin-up electrons is drastically different from that of the spin-down electrons in the broad energy range [−1.67 eV, 0.70 eV]. Particularly around the Fermi level, the transmission of the spin-up electrons shows a broad transmission dip centered at around −0.25 eV, whereas a relatively sharp transmission dip for the spin-down electrons appears only at 0.36 eV. Once again, these spin-resolved transport characteristics can find their origin in the DOS of the Ni adatom (see Fig. 6(b)). For the spin-up electrons, the $3d_{yz}$ and $3d_{xz}$ atomic orbitals form a sharp peak at 0.50 eV below E_F together with a small shoulder at −0.23 eV, and also contribute to the sharp peak centered at −1.21 eV. In contrast, for the spin-down electrons the $3d_{yz}$ and $3d_{xz}$ atomic orbitals of the Ni adatom only dominate the DOS peak centered at around −0.97 eV, while the DOS peak at 0.33 eV above E_F is mainly due to the Ni 4p atomic orbitals.

Undoubtedly, all of the spin-features are caused by the adsorption of the nickelocene molecule. Nickelocene in the gas phase has a spin moment of $2\mu_B$, since Ni has one valence electron more than Co. This means that the doubly degener-

ate, doubly occupied molecular orbital dominated by the Ni $3d_{yz}$ and $3d_{xz}$ atomic orbitals is the highest occupied molecular orbital for the spin-up electrons, while it is the lowest unoccupied molecule orbital for the spin-down electrons.[18] The nickelocene molecule retains the spin polarization even after it adsorbs onto the nanotube. The spin-resolved DOS of the nickelocene nickel center is shown in Fig. 6(c). The Ni $3d_{yz}$ and $3d_{xz}$ atomic orbitals form three spin-up peaks located, respectively, at 1.46 eV, 1.20 eV, and 0.50 eV below E_F. It is worth noting that both the energy position and the overall shape of the DOS at −0.50 eV for the nickel center are identical to the same peak of the Ni adatom. In contrast, the Ni $3d_{yz}$ and $3d_{xz}$ atomic orbitals mainly contribute a spin-down DOS peak at about 0.33 eV above the Fermi level, though also the small DOS peak at −0.97 eV is contributed by the same.

Here, we would like to discuss the effects that self-interaction corrections (SIC) may have on the calculated spin transport properties of metallocene molecules adsorbed on the SWCNT, and cobaltocene is selected as the representative example for the metallocenes. It is well known that molecular levels calculated by using local and semi-local exchange and correlation functionals (local density approximation, LDA, or GGA) are too shallow (too high in energy) due to the self-interaction error.[47] This may result in an incorrect alignment of molecular levels with the Fermi energy of the electrodes and thus an unphysical transmission peak or dip at around E_F. It is therefore interesting to explore whether or not the calculated transmission dips around the Fermi level for the spin-up channel of the (4,4) SWCNT adsorbed with the cobaltocene molecule (Fig. 5(a)) is genuine or simply an artifact of the self-interaction error contained in the PBE GGA functional. The atomic self-interaction correction (ASIC) scheme[48] applied to the non-equilibrium quantum transport problem[49–52] is used to carry out this analysis. The ASIC corrections are applied to the cobaltocene molecule and the Ni adatom, not to the carbon atoms in the (4,4) SWCNT as self-interaction errors for metals are small. The empirical scale factor α, which is a measure of the deviation of the ASIC potential from the exact SIC one, is set to be 0.0 (LDA limit), 0.25, and 0.5. Since our ASIC method is based on the Perdew-Zunger (PZ) LDA functional,[53] we first compare the spin-resolved transmission coefficients of the (4,4) armchair SWCNT adsorbed with a cobaltocene molecule as calculated by using PZ LDA with those obtained previously with PBE GGA (see Fig. 7). As we can see, the overall shape of these transmission curves is similar. The only exception is for the fact that the transmission dip around 0.72 eV for the spin-down electrons calculated by using PBE moves to above 1.2 eV (not shown here) when the PZ LDA functional is used. The reason for this occurrence is that the spin-down DOS peak dominated by the Co $3d_{yz}$ and $3d_{xz}$ atomic orbitals is shifted from about 0.76 eV for PBE to above 1.2 eV for PZ. When α is increased from 0 to 0.5, the transmission curves for both the spin-up and spin-down channels around the Fermi level change slightly with the position of the transmission dips moving downwards in energy. Thus, for the cobaltocene molecule attached to the (4,4) SWCNT sidewall the SIC does not alter qualitatively the spin transport properties around the Fermi level.

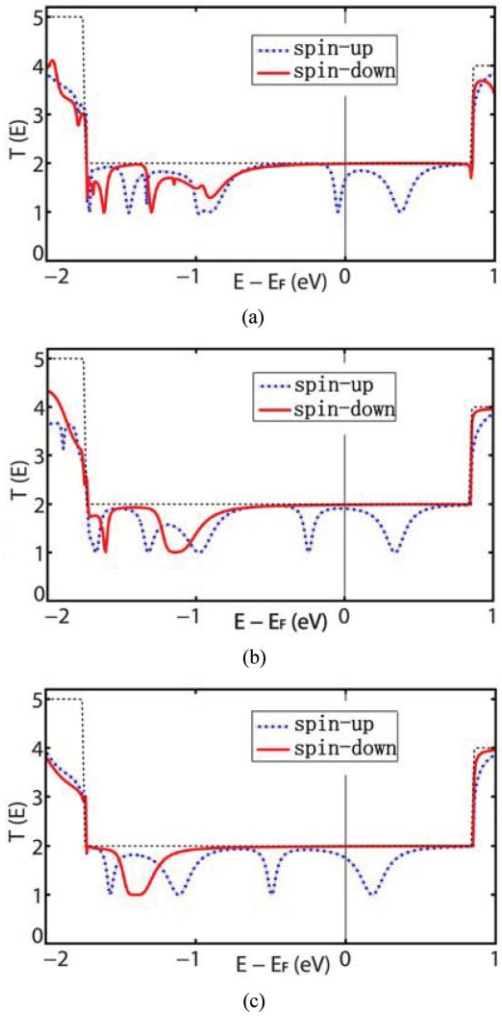

FIG. 7. Spin transport properties of a (4,4) armchair SWCNT with a cobaltocene molecule adsorbed at its sidewall through a Ni adatom calculated by using the ASIC method with different scaling factors : (a) $\alpha = 0.0$ (LDA); (b) $\alpha = 0.25$; and (c) $\alpha = 0.5$.

Since we are interested in engineering the spin filtering properties of the metallocene/SWCNT systems, our primary aim is that of finding a molecule producing the largest possible difference between the transmission coefficients of the spin-up and spin-down channels around the Fermi level. In contrast to nickelocene, the adsorption of cobaltocene onto the sidewall of the (4,4) armchair SWCNT introduces two transmission dips in the spin-up channel around the Fermi level, but does not alter the transmission of the spin-down one. Furthermore, these two transmission dips always straddle the Fermi level even when the SIC functional is considered, demonstrating the superiority of cobaltocene over other metallocenes in spin filtering the low-bias current. Certainly placing a single metallocene molecule exactly above the Ni adatom adsorbed on the sidewall of a SWCNT appears as a difficult practical task. One possible way for realizing such a device configuration is that of using scanning tunneling microscope (STM) atomic manipulation. It has been demonstrated that STM is capable of imaging and manipulating single molecules with atomic resolution, thus one can use the STM tip to move a metallocene molecule onto the Ni adatom adsorbed at the nanotube sidewall. STM manipulation

may, however, be time-consuming and ultrahigh vacuum, low temperature, and a combination of other conditions may be needed. Of course, there may also be a chemical way to synthesize our proposed composite material, which has not been pursued so far. We hope that our work will inspire such a synthetic effort.

IV. CONCLUSION

In this work, we have investigated the spin-dependent transport properties of single metallocene molecules attached to the sidewall of the (4,4) armchair SWCNT through a single nickel adatom. Ni adsorbed at the outside atop site provides an excellent linkage for metallocene molecules. Since neither the spin degeneracy nor the transmission coefficient around the Fermi level of the (4,4) SWCNT is disturbed by the Ni adatom, any changes in the transport characteristics originate from the metallocene molecules attached to it. In contrast to ferrocene, both cobaltocene and nickelocene are able to cause the spin-dependent blocking of a conducting channel at certain energies around E_F. The exact details of such a modification of the nanotube transmission spectrum are rooted in the interaction of the metallocene molecule with the linking Ni adatom. In particular, we always find that fingerprints of the DOS of the particular metallic center in metallocene appear in the transmission. This allows one to modify the spin-polarization of the current in the nanotube by simply attaching a magnetic adsorbate to it. We have further demonstrated that such an attachment is robust, since the binding energies of the Ni adatom, cobaltocene, and nickelecene molecules are all calculated to be in the 2 eV range. Thus, the combination of metallocene molecules and SWCNTs appears promising for the construction of molecular spintronic devices with tunable spin transport properties and high thermal stability.

ACKNOWLEDGMENTS

This project was supported by the National Natural Science Foundation of China (No. 61071012), the Ministry of Education (NCET-07-0014), and the MOST of China (Nos. 2007CB936204 and 2011CB933001). The SMEAGOL project (SS) is sponsored by the Science Foundation of Ireland (07/IN.1/I945) and by CRANN.

[1] S. Sanvito, J. Mater. Chem. **17**, 4455 (2007); Chem. Soc. Rev. **40**, 3336 (2011).
[2] L. Bogani and W. Wernsdorfer, Nature Mater. **7**, 179 (2008).
[3] N. Baadji, M. Piacenza, T. Tugsuz, F. Della Sala, G. Maruccio, and S. Sanvito, Nature Mater. **8**, 813 (2009).
[4] H. Dai, *Nanotube Growth and Characterization, Carbon Nanotubes*, edited by M. S.Dresselhaus, G. Dresselhaus, and P. Avouris (Springer, Berlin, 2001).
[5] X. Guo, J. P. Small, J. E. Klare, Y. Wang, M. S. Purewal, I. W. Tam, B. H. Hong, R. Caldwell, L. Huang, S. O'Brien, J. Yan, R. Breslow, S. J. Wind, J. Hone, P. Kim, and C. Nuckolls, Science **311**, 356 (2006).
[6] X. Guo, A. A. Gorodetsky, J. Hone, J. K. Barton, and C. Nuckolls, Nat. Nanotechnol. **3**, 163 (2008).
[7] X. Guo, S. Xiao, M. Myers, Q. Miao, M. L. Steigerwald, and C. Nuckolls, Proc. Natl. Acad. Sci. U.S.A. **106**, 691 (2009).
[8] P. Qi, A. Javey, M. Rolandi, Q. Wang, E. Yenilmez, and H. Dai, J. Am. Chem. Soc. **126**, 11774 (2004).
[9] F. S. M. Guimarães, D. F. Kirwan, A. T. Costa, R. B. Muniz, D. L. Mills, and M. S. Ferreira, Phys. Rev. B **81**, 153408 (2010).
[10] L. Bogani and W. Wernsdorfer, Inorg. Chim. Acta **361**, 3807 (2008).
[11] V. V. Maslyuk, A. Bagrets, V. Meded, A. Arnold, F. Evers, M. Brandbyge, T. Bredow, and I. Mertig, Phys. Rev. Lett. **97**, 097201 (2006).
[12] H. Xiang, J. Yang, J. G. Hou, and Q. Zhu, J. Am. Chem. Soc. **128**, 2310 (2006).
[13] M. Koleini, M. Paulsson, and M. Brandbyge, Phys. Rev. Lett. **98**, 197202 (2007).
[14] L. Wang, Z. Cai, J. Wang, J. Lu, G. Luo, L. Lai, J. Zhou, R. Qin, Z. Gao, D. Yu, G. Li, W. N. Mei, and S. Sanvito, Nano Lett. **8**, 364 (2008).
[15] L. Zhou, S. W. Yang, M. F. Ng, M. B. Sullivan, V. B. C. Tan, and L. Shen, J. Am. Chem. Soc. **130**, 4023 (2008).
[16] L. Shen, S. W. Yang, M. F. Ng, V. Ligatchev, L. Zhou, and Y. Feng, J. Am. Chem. Soc. **130**, 13956 (2008).
[17] X. Shen, Z. Yi, Z. Shen, X. Zhao, J. Wu, S. Hou, and S. Sanvito, Nanotechnology **20**, 385401 (2009).
[18] Z. Yi, X. Shen, L. Sun, Z. Shen, S. Hou, and S. Sanvito, ACS Nano **4**, 2274 (2010).
[19] C. Morari, A. R. Rocha, S. Sanvito, S. Melinte, and G.-M. Rignanese, ACS Nano **3**, 4137 (2009).
[20] X. Shen, L. Sun, E. Benassi, Z. Shen, X. Zhao, S. Sanvito, and S. Hou, J. Chem. Phys. **132**, 054703 (2010).
[21] X. Shen, L. Sun, Z. Yi, E. Benassi, R. Zhang, Z. Shen, S. Sanvito, and S. Hou, Phys. Chem. Chem. Phys. **12**, 10805 (2010).
[22] Y. Meir and N. S. Wingreen, Phys. Rev. Lett. **68**, 2512 (1992).
[23] P. Hohenberg and W. Kohn, Phys. Rev. **136**, B864 (1964).
[24] W. Kohn and L. J. Sham, Phys. Rev. **140**, A1133 (1965).
[25] Y. Xue, S. Datta, and M. A. Ratner, Chem. Phys. **281**, 151 (2002).
[26] M. Brandbyge, J.-L. Mozos, P. Ordejón, J. Taylor, and K. Stokbro, Phys. Rev. B **65**, 165401 (2002).
[27] J. Zhang, S. Hou, R. Li, Z. Qian, R. Han, Z. Shen, X. Zhao, and Z. Xue, Nanotechnology **16**, 3057 (2005).
[28] R. Li, J. Zhang, S. Hou, Z. Qian, Z. Shen, X. Zhao, and Z. Xue, Chem. Phys. **336**, 127 (2007).
[29] A. R. Rocha, V. M. Garcia-Suarez, S. W. Bailey, C. J. Lambert, J. Ferrer, and S. Sanvito, Nature Mater. **4**, 335 (2005).
[30] A. R. Rocha, V. M. García-Suárez, S. Bailey, C. Lambert, J. Ferrer, and S. Sanvito, Phys. Rev. B **73**, 085414 (2006).
[31] I. Rungger and S. Sanvito, Phys. Rev. B **79**, 035407 (2008).
[32] D. M. Guldi, M. Marcaccio, D. Paolucci, F. Paolucci, N. Tagmatarchis, D. Tasis, E. Vázquez, and M. Prato, Angew. Chem., Int. Ed. **42**, 4206 (2003).
[33] J. M. Soler, E. Artacho, J. D. Gale, A. García, J. Junquera, P. Ordejón, and D. Sánchez-Portal, J. Phys.: Condens. Matter **14**, 2745 (2002).
[34] N. Troullier and J. Martins, Phys. Rev. B **43**, 1993 (1991).
[35] J. Perdew, K. Burke, and M. Ernzerhof, Phys. Rev. Lett. **77**, 3865 (1996).
[36] S. F. Boys and F. Bernardi, Mol. Phys. **19**, 553 (1970).
[37] Z. Qian, S. Hou, J. Ning, R. Li, Z. Shen, X. Zhao, and Z. Xue, J. Chem. Phys. **126**, 084705 (2007).
[38] J. M. Carcía-Lastra, K. S. Thygesen, M. Strange, and A. Rubio, Phys. Rev. Lett. **101**, 236806 (2008).
[39] Y. Yagi, T. M. Briere, M. H. F. Sluiter, V. Kumar, A. A. Farajian, and Y. Kawazoe, Phys. Rev. B **69**, 075414 (2004).
[40] J. A. Fürst, M. Brandbyge, A.-P. Jauho, and K. Stokbro, Phys. Rev. B **78**, 195405 (2008).
[41] R. Saito, G. Dresselhaus, and M. S. Dresselhaus, *Physical Properties of Carbon Nanotubes* (Imperial College Press, London, 1998).
[42] P. Delaney, H.-J. Choi, J. Ihm, S. G. Louie, and M. L. Cohen, Nature (London) **391**, 466 (1998).
[43] M. Paulsson and M. Brandbyge, Phys. Rev. B **76**, 115117 (2007).
[44] S. Hou, Y. Chen, X. Shen, R. Li, J. Ning, Z. Qian, and S. Sanvito, Chem. Phys. **354**, 106 (2008).
[45] R. Li, S. Hou, J. Zhang, Z. Qian, Z. Shen, and X. J. Zhao, J. Chem. Phys. **125**, 194113 (2006).
[46] K. H. Khoo and J. R. Chelikowsky, Phys. Rev. B **79**, 205422 (2009).
[47] W. Koch and M. C. Holthausen, *A Chemist's Guide to Density Functional Theory*, 2nd ed. (Wiley VCH, Weinheim, 2001).
[48] C. D. Pemmaraju, T. Archer, D. Sánchez-Portal, and S. Sanvito, Phys. Rev. B **75**, 045101 (2007).
[49] C. Toher and S. Sanvito, Phys. Rev. Lett. **99**, 056801(2007).
[50] C. Toher and S. Sanvito, Phys. Rev. B **77**, 155402 (2008).
[51] G. Ma, X. Shen, L. Sun, R. Zhang, P. Wei, S. Sanvito, and S. Hou, Nanotechnology **21**, 495202 (2010).
[52] R. B. Pontes, A. R. Rocha, S. Sanvito, A. Fazzio, and A. J. R. da Silva, ACS Nano **5**, 795 (2011).
[53] J. P. Perdew and Z. Zunger, Phys. Rev. B **23**, 5048 (1981).